



HAL
open science

Deciphering the Unexpected Binding Capacity of the Third PDZ Domain of Whirlin to Various Cochlear Hair Cell Partners

Yanlei Zhu, Florent Delhommel, Florence Cordier, Susanne Lüchow, Ariel E Mechaly, Baptiste Colcombet-Cazenave, Virginie Girault, Elise Pepermans, Amel Bahloul, Candice Gautier, et al.

► **To cite this version:**

Yanlei Zhu, Florent Delhommel, Florence Cordier, Susanne Lüchow, Ariel E Mechaly, et al.. Deciphering the Unexpected Binding Capacity of the Third PDZ Domain of Whirlin to Various Cochlear Hair Cell Partners. *Journal of Molecular Biology*, 2020, 432 (22), pp.5920 - 5937. 10.1016/j.jmb.2020.09.012 . hal-02990253

HAL Id: hal-02990253

<https://hal.science/hal-02990253>

Submitted on 17 Nov 2020

HAL is a multi-disciplinary open access archive for the deposit and dissemination of scientific research documents, whether they are published or not. The documents may come from teaching and research institutions in France or abroad, or from public or private research centers.

L'archive ouverte pluridisciplinaire **HAL**, est destinée au dépôt et à la diffusion de documents scientifiques de niveau recherche, publiés ou non, émanant des établissements d'enseignement et de recherche français ou étrangers, des laboratoires publics ou privés.



Distributed under a Creative Commons Attribution - NonCommercial 4.0 International License

Deciphering the unexpected binding capacity of the third PDZ domain of whirlin to various cochlear hair cell partners

Yanlei ZHU^{1,2}, Florent DELHOMMEL^{1,2,8}, Florence CORDIER³, Susanne LÜCHOW⁴, Ariel MECHALY⁵, Baptiste COLCOMBET-CAZENAVE^{1,2}, Virginie GIRAULT^{1,9}, Elise PEPERMANS^{2,10,11}, Amel BAHLOUL^{10,12}, Candice GAUTIER⁶, Sébastien BRULE⁷, Bertrand RAYNAL⁷, Sylviane HOOS⁷, Ahmed HAOUZ⁵, Célia CAILLET-SAGUY¹, Ylva IVARSSON⁴, Nicolas WOLFF^{1*}

¹Unité Récepteurs-Canaux, Institut Pasteur, 75015 Paris, France

²Complexité du Vivant, Sorbonne Université, 75005 Paris, France

³Unité de Bioinformatique Structurale, 75015 Paris, France

⁴Department of Chemistry-BMC, Uppsala University, Sweden

⁵Plateforme de Cristallographie, Institut Pasteur, Paris, France.

⁶Istituto Pasteur - Fondazione C. Bolognetti, Sapienza Università di Roma, Rome, Italy

⁷Plateforme de Biophysique Moléculaire, Institut Pasteur, Paris, France.

⁸Current address: Institute of Structural Biology, Helmholtz Zentrum München, Germany

⁹Current address: Institute of Virology, Technical University of Munich, Germany,

¹⁰Unité de génétique et physiologie de l'audition, Institut Pasteur, 75015 Paris, France

¹¹Current address: Center for proteomics, University of Antwerp, 2020 Antwerp, Belgium

¹²Current address: Department of otolaryngology - Head and neck surgery, Stanford university, Stanford, California, USA.

*Corresponding author. E-mail: nicolas.wolff@pasteur.fr

Highlights

- The third PDZ domain of whirlin is independent in the multi-domain organization of the Usher protein

- PDZ3 of whirlin recognizes at least seven stereociliary proteins
- Whirlin PDZ3 can bind both canonical and internal PDZ binding motifs
- Whirlin interacts with CASK/MPP1 kinases through a new PDZ-PBM recognition mode
- A unique 'Lys-Phe lock' increases the rigidity of the PDZ3 binding groove

Summary

Hearing is a mechanical and neurochemical process, which occurs in the hair cells of inner ear that converts the sound vibrations into electrical signals transmitted to the brain. The multi-PDZ scaffolding protein whirlin plays a critical role in the formation and function of stereocilia exposed at the surface of hair cells. In this article, we reported seven stereociliary proteins that encode PDZ binding motifs (PBM) and interact with whirlin PDZ3, where four of them are first reported. We solved the atomic resolution structures of complexes between whirlin PDZ3 and the PBMs of myosin 15a, CASK, harmonin a1 and taperin. Interestingly, the PBM of CASK and taperin are rare non-canonical PBM, that are not localized at the extreme C-terminus. This large capacity to accommodate various partners could be related to the distinct functions of whirlin at different stages of the hair cell development.

Key words

Whirlin, Usher proteins, PDZ domain, stereocilium

Introduction

1 The sense of hearing is a mechanical and neurochemical process that requires
2 highly specialized sensory cells (inner and outer hair cells) in the cochlea of the inner
3 ear. At their apical surfaces, three rows of staircase-like actin-filled stereocilia are
4 connected by different types of extracellular links. Two unconventional cadherins,
5 protocadherin 15 (USH1F) and cadherin 23 (USH1D) form the interstereociliary tip link
6 of auditory hair cell bundles, that conveys sound-evoked forces to the cation transducer
7 channels [1][2]. These links are required to perform the mechanoelectrical transduction
8 of the sound-induced vibrations [3][4][5][6]. During hair cell development, the hair
9 bundle also harbours transient links called ankle links located at the stereocilia base.
10 Both tip links and ankle links are anchored to large protein complex in the
11 submembrane region. Most of the proteins that form these anchoring densities are
12 called Usher proteins, as mutations altering their function cause the Usher syndrome
13 (USH), that is the most common form of hereditary hearing-vision loss in humans. Usher
14 proteins play fundamental roles in maintaining the particular sub-cellular structures
15 and functions of hearing [7][8][9][4], and same proteins are also found in retina
16 photoreceptor cells. The submembrane scaffold proteins harmonin (USH1C) and SANS
17 (Scaffolds protein containing Ankyrin repeats and SAM domain) (USH1G) anchor the
18 upper part of this tip link to actin filaments directly or through interactions mediated by
19 the actin-binding protein myosin 7a (USH1B). Usherin (USH2A) and ADGRV1
20 (USH2C)(adhesion G protein-coupled receptor V1). the two other large transmembrane
21 Usher proteins make part of the ankle link complex [10] and are associated to the PDZ-
22 scaffold proteins whirlin (USH2D) and PDZD7 (DFNB57) in the cytoplasm.

23 Whirlin is a multi-domain scaffolding protein, which is essential for the bundling
24 and growing of stereocilia of the hair cells [7][11]. Human whirlin is composed of 907
25 amino acids and encompasses two harmonin Homology Domains (HHD)[12], three PDZ
26 domains, a proline-rich (PR) region and a C-terminal PBM (PDZ binding motif)
27 (Fig.1)(Mburu et al., 2003). Whirlin is expressed in three main isoforms. The full-length
28 (FL) isoform is found in both retina photoreceptor cells and auditory hair cells, which is
29 an important component of the transient ankle links complex during development, and
30 FL isoform has also been found at the tips of the tallest row of stereocilia [13]. The C-
31 terminal isoform including the region from HHD2 to the C-terminal PBM is required for
32 normal stereocilia length regulation, and is only expressed at the tips of tallest row of
33 stereocilia [14][15] [13][16]. Besides the Usher syndrome, the mutations in the C-
34 terminal isoform region can also lead to non-syndromic deafness (DFNB31). Finally, the
35 N-terminal isoform contains the N-terminal HHD1, a tandem of PDZ domains (PDZ1-2)
36 and a second HHD domain (HHD2) but is only expressed in retina cells [7][8][9].

37 Considering the various localizations of the protein according to the stages of
38 development of hair bundle, whirlin is expected to participate in dynamical and
39 transient complexes in rather different cellular environments. At the ankle links, whirlin
40
41
42
43
44
45
46
47
48
49
50
51
52
53
54
55
56
57
58
59
60
61
62
63
64
65

1
2
3
4
5
6
7
8
9
10
11
12
13
14
15
16
17
18
19
20
21
22
23
24
25
26
27
28
29
30
31
32
33
34
35
36
37
38
39
40
41
42
43
44
45
46
47
48
49
50
51
52
53
54
55
56
57
58
59
60
61
62
63
64
65
interacts with usherin and ADGRV1, the two proteins critical for formation of these inter-stereocilia links [17]. At the tip of tall stereocilia, whirlin controls the polymerization of F-actin, most likely together with others proteins such as EPS8 (epidermal growth factor receptor pathway substrate 8), myosin 15a and GPSM2 (G-protein signalling modulator 2) [18][14][15][19]. In the photoreceptor cells, SANS, usherin and whirlin have been reported to form a ternary complex [20]. Whirlin has been found enriched at inner segments and ciliary region but also distributed throughout the whole photoreceptor cells just like the harmonin a isoform [20] [21].

The PDZ domains of whirlin play a pivotal role in organizing these protein networks. PDZ domains are small modules of about 90 amino acids folded into five to six β -strands and one to two α -helices. The PDZ domain canonically recognizes short motifs composed of the last three C-terminal residues of the partners, known as PDZ Binding Motif (PBM). The C-terminus carboxylate of the motif directly contacts to the β 1- β 2 loop or 'GLGF' loop that is a main PDZ-PBM binding feature [22]. The two N-terminal PDZ domains of whirlin form a supramodule that enables fine-tuning of affinities for Usher proteins such as SANS and usherin [23][12]. The third PDZ domain of whirlin, present in both the FL and C-terminal isoforms, has been shown to interact with several partners but the molecular details of these interactions are not known. Whirlin PDZ3 binds to the class I canonical PBM of myosin 15a and participates to the F-actin polymerisation in a molecular complex at the stereocilia tip [14] [18]. Early reports have also described whirlin is expressed in neuron cell soma and dendrites of the central nervous system; where its interaction with the Calcium/Calmodulin Dependent Serine Protein Kinase (CASK) has been confirmed [24]. In hair cells, the MAGUK proteins CASK and MPP1 (Membrane Palmitoylated Protein 1) have been shown to colocalize with whirlin [25][26]. Interestingly, the last 10 residues of CASK and MPP1 are identical and contain an internal class I PDZ binding motif (PBM) (-S-W-V-Y) albeit not at the C-terminus but shifted by one residue.

In this study, we characterize at the molecular level the interaction of the whirlin PDZ3 domain with its different cellular partners. We identified harmonin a1 and taperin as interacting partners of this domain, using an *in vitro* high throughput *Holdup* assay [27] and a proteomic peptide phage display (ProP-PD; PMID: 28002650), respectively. We also characterized the PDZ mediated interactions using a number of biophysical methods and solved the X-ray structures of whirlin PDZ3 in complex with four of its binding partners: myosin 15a, CASK, harmonin a1 and taperin. The comparison of these high-resolution structures highlights the plasticity of interaction of whirlin PDZ3, which is able to interact with several divergent PDZ binding motifs. These results extend our understanding of the binding plasticity of PDZ domains and further confirm the multiple roles of whirlin in the development of sensory cells and its relation with non-syndromic deafness (DFNB31).

Results

The C-terminal region of whirlin adopts an extended form with independent folded domains HHD2 and PDZ3

In the full-length protein and the short C-terminal isoform of whirlin (starting from HHD2 to PBM), the third PDZ domain is localized at the C-terminal end of the protein and linked to the HHD2 domain through a sequence of 309 residues including a proline rich (PR) region. As illustrated by the IUPRED plot (<https://iupred2a.elte.hu>;[28]) (Fig. 1), this large linker region is predicted to be intrinsically disordered and tethers the two well-defined folded structures of HHD2 domain and PDZ3 domain [29].

We investigated the conformation of several constructs of the C-terminal isoform using small angle X-ray scattering (SAXS) (Fig. 1). We produced five constructs of the C-terminal isoform; the proline rich region (PR), the second HHD domain (HHD2), the third PDZ domain (PDZ3), a segment from the PR region to the PDZ3 domain (PR-PDZ3) and a segment from the second HHD to the PR (HHD2-PR). The Guinier approximation of the radius of gyration at low q value and maximum distance values (D_{max}) estimated from the pair-distance distribution function showed that the PR constructs corresponding to the large inter-domain linker yields a large radius of gyration (R_g , 57.1 Å) and a maximum distance of 250 Å. Similarly, for the constructs PR, PR-PDZ3 and HHD2-PR, large values of R_g and D_{max} are found, which is consistent with the presence of a large flexible sequence that links the folded domains. By contrast, the two globular single domains HHD2 and PDZ3 showed much smaller R_g and D_{max} values in agreement with their molecular weights. The dimensionless Kratky plot provides a sensitive means to evaluate the degree of compactness of proteins; interestingly, the PR region behaves in solution as an extended and flexible sequence with a plateau at large q -values while HHD2 and PDZ3 adopt folded and compact conformations as represented by their bell-shaped curves (Fig. 1).

Previously we reported the HHD2 domain does not interact with the N-terminal PDZ1 and PDZ2 domains and binding partners of the HHD2 are currently unknown [29]. Overall, our results demonstrated that the PDZ3 domain is independent from the other folded domain HHD2, in the larger molecular context of whirlin as it is linked to the rest of the molecule by flexible sequence. It is therefore useful to study this domain as an independent feature of the whirlin.

1
2
3
4
5
6
7
8
9
10
11
12
13
14
15
16
17
18
19
20
21
22
23
24
25
26
27
28
29
30
31
32
33
34
35
36
37
38
39
40
41
42
43
44
45
46
47
48
49
50
51
52
53
54
55
56
57
58
59
60
61
62
63
64
65

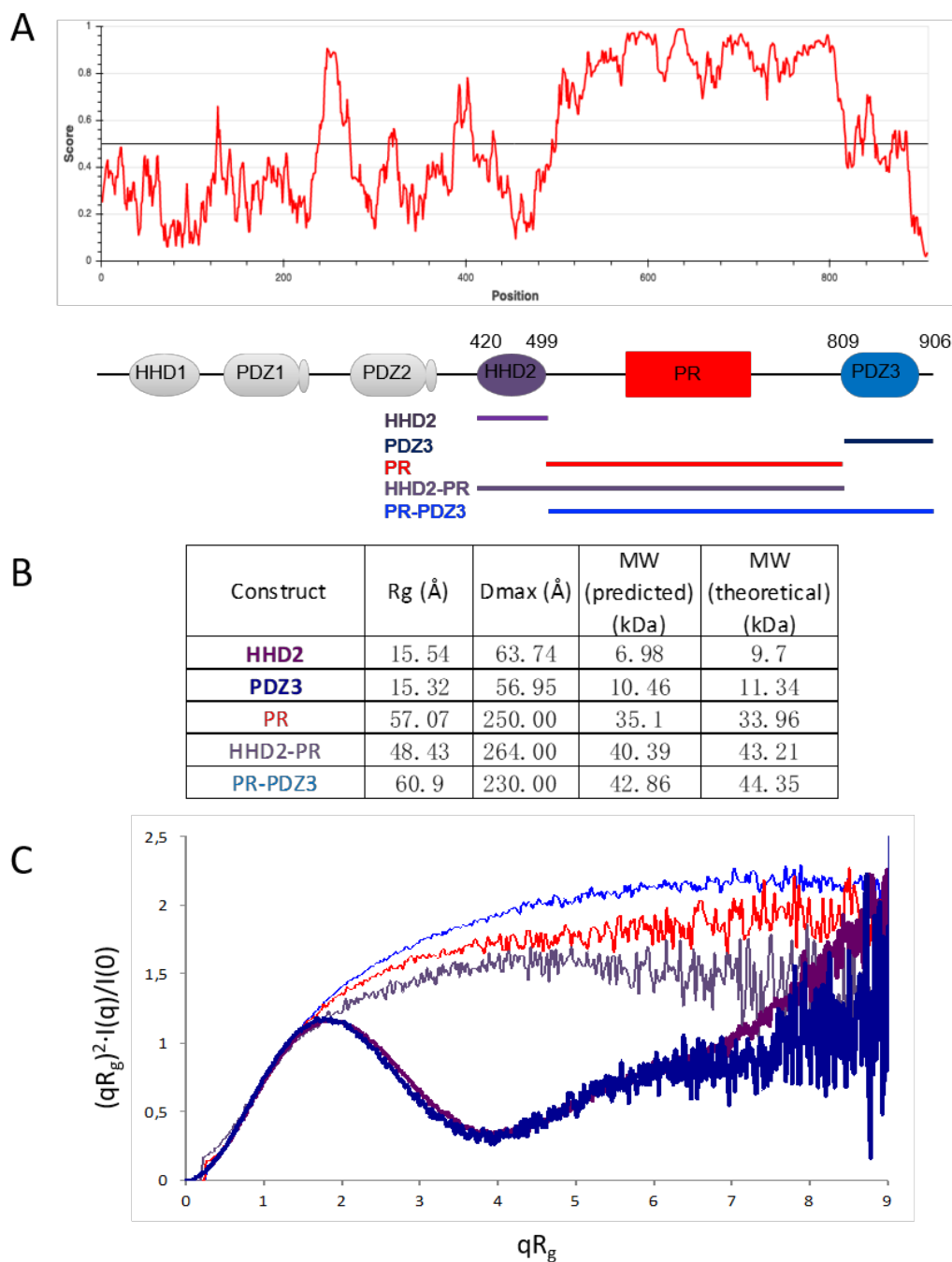


Figure 1: PDZ3 domain is separated by a long proline rich region (PR) from N-terminal domains. A: The IUPRED predicted structured and unstructured regions of FL-whirlin. The five generated constructs are underlined (sequence based on Uniprot ID Q80VW5-4). B: size parameters Rg and Dmax extracted from SAXS data, and predicted and theoretical molecular weight (MW) for whirlin constructs. C: dimensionless Kratky plots of PR involved constructs. Five constructs are in the same colours in Fig 1A and 1B.

The PDZ3 domain of whirlin recognizes the PBM sequences of harmonin a1 and taperin as two newly identified binders

Using *in vitro* high-throughput approaches, we identified PDZ3 binding partners. Short peptides encompassing a biotinyl group, a (PEG)₃ spacer and the C-terminal PBM sequence of Usher proteins (11 to 16 residues long) were synthesized. These peptides were used as bait in the automated high-throughput chromatography assay *Holdup* which allowed to quantify the interaction between the whirlin PDZ3 domain and the collection of stereociliary protein PBMs [27]. The *Holdup* approach displayed a high sensitivity for low to medium-affinity pairs and presented the unique advantage of providing affinity-based ranking of the identified binders. Results are showed in binding intensities (BI) (Table 1), a measure of binding that correlates directly to the affinity of interaction that is comprised between 0 for no interaction and 1 for all observed species bound. The PBM of harmonin a1, myosin 15a and cadherin23 displayed significant BI values higher than 0.2, an empirical threshold defining relevant from unspecific interactions. (Table 1) [27]. We concluded here that the PBM sequences of harmonin a1, myosin 15a and cadherin23 proteins have the capacity to bind to PDZ3 *in vitro* in the 1-100 μM affinity range typically found for PDZ/PBM interactions. The third isoform of protocadherin 15 (CD3) shows a BI slightly above threshold, suggesting a possible weak interaction. We then quantified by surface plasmonic resonance (SPR) the interactions between PDZ3 and the PBMs of these Usher proteins. *Holdup* and SPR data were in perfect agreement. The ranking of affinity between the two methods are fully consistent. Among the PBM-containing Usher proteins, only myosin 15a, cadherin 23, harmonin a1 and protocadherin 15-CD3 are binders of PDZ3 with affinities ranging from 5 to 250 μM .

Table 1: Measured affinities between the whirlin PDZ3 domain and the collection of stereociliary protein PBMs. A: *Holdup* assay results are reported as Binding Intensities (BI) which correlate with binding affinities scale [27]. B: Surface Plasmon Resonance (SPR) data are reported as K_d (μM).

PBM peptides	<i>Holdup</i> (BI)	K_d by SPR (μM)
myosin 15a	0.67	4.4±0.8
cadherin 23	0.57	4.3±0.3
harmonin a1	0.45	67±25
protocadherin15-CD3	0.26	230±30
SANS	0.19	No Binding
whirlin	0.03	No Binding
protocadherin15-CD2	0.01	No Binding
protocadherin15-CD1	-0.03	No Binding
ADGRV1	-0.03	No Binding
usherin	-0.05	No Binding

1 We identified partners of whirlin from the apical complexes in hair cells. To
2 enlarge the panel of whirlin binders, we explore the capacity of its PDZ3 to recognize
3 internal PDZ binding motifs. Some PDZ domains have been reported to also interact with
4 non-canonical PDZ binding motifs that are found in intrinsically disordered regions of
5 target proteins [30][31][32]. We used a previously described phage library that present
6 a peptidome that covers the intrinsically disordered regions of the human proteome
7 [33]. The displayed peptides are 16 amino acids long, and the library design comprises
8 about 500,000 unique peptides. MBP-tagged whirlin PDZ3 was used as bait protein for
9 five cycles of phage display selection. Phage pool ELISA confirmed that there was an
10 enrichment of binders over the days of selection. The peptide-coding region of the
11 resulting binding enriched phage pool was analysed through next-generation
12 sequencing (NGS). The analysis revealed that a single peptide from the inner ear
13 stereocilia protein, taperin, was highly enriched. Taperin (DFNB79) is a non-syndromic
14 deafness protein expressed at the base of stereocilia, which is critical for the length and
15 orientation of stereocilia [34][35][36]. The PDZ3 domain of whirlin is thus capable of
16 binding internal ligands, and likely with high specificity. Analysis of the taperin peptide
17 sequence (LPV**T**FIDEVDSEEAPQ) identified a putative internal class I binding motif
18 followed by acidic residues.
19
20
21
22
23
24
25
26
27
28

29 ***Affinity determination of whirlin PDZ3 domain with various PBM cellular partners***

30 Besides the high-throughput methods, we determined the affinities of the four PBM
31 sequences of CASK, myosin 15a, harmonin a1, and taperin for the PDZ3 domain using
32 NMR and fluorescence titrations for better understanding of structural information. By
33 NMR titration, K_d values of the interactions between PDZ3 and myosin 15a and
34 harmonin a1 were determined following ^1H , ^{15}N chemical shift perturbations of about 15
35 resonances in the ^1H - ^{15}N HSQC spectra as a function of increasing concentrations of the
36 PBM-containing peptide. The binding affinity with myosin 15a peptide is $2.9 \pm 1.6 \mu\text{M}$,
37 the strongest value among the four binding partners, while harmonin a1 peptide is the
38 weakest binding partner with a K_d value 45-fold lower at $132 \pm 13 \mu\text{M}$. This K_d value is in
39 the lower range of affinity commonly found for PDZ domain interactions. For taperin,
40 the K_d was determined by following the variation of the bound signal intensity because
41 of the slow exchange binding process with this peptide. An affinity of $58 \pm 31 \mu\text{M}$ (Table
42 2) was estimated for taperin. For CASK, the slow/intermediate exchange regime
43 observed in the NMR spectra led to severe line broadening during the course of titration
44 and prevented an accurate K_d measurement. Therefore, we used fluorescence titration,
45 following the emission fluorescence intensity of the unique tryptophan of the CASK
46 peptide (-SWVY_{COOH}) affected by the binding to the PDZ3 domain. The K_d value is $7.1 \pm$
47 $1.0 \mu\text{M}$ for the CASK peptide, similar to the one obtained with the myosin 15a peptide.
48
49
50
51
52
53
54
55
56
57
58
59
60
61
62
63
64
65

The PDZ3 domain is tethered to the C-terminal PBM of whirlin –VML_{COOH} by a short linker of three residues. In order to evaluate if the PBM sequence of whirlin can affect the intermolecular binding properties of PDZ3 to its partner, we compared the affinity of PDZ3 and PDZ3 deleted from the PBM (PDZ3ΔPBM) for myosin 15a, which is the best binder. The K_d values of myosin 15a are similar for PDZ3ΔPBM and PDZ3 with 3.4 ± 1.8 μM and 2.9 ± 1.6 μM, respectively. We concluded that the whirlin PBM does not interfere with the binding of partner to the PDZ3 domain.

Table 2: Binding affinity of PDZ3 to various PBMs with sequences and binding pattern. The three residues that form the PBM are in bold. *: The CASK K_d value was determined using fluorescence titration, and others were measured by NMR titration.

	Peptide	Sequence	K _d (μM)	binding pattern
PDZ3ΔPBM	myosin 15a	ERLTLPPSEIT LL	3.4 ± 1.8	Class I
PDZ3	myosin 15a	ERLTLPPSEIT LL	2.9 ± 1.6	Class I
PDZ3	harmonin a1	PKEYDDEL TFF	132 ± 13	Class I
PDZ3	CASK*	TAPQWVPV SWVY	7.1 ± 1.0	Class I (internal PBM)
PDZ3	taperin	GLPVT FIDEVD SEEAPQ	58 ± 31	Class I (internal PBM)

High resolution structures of PDZ3 complexes

Overall structure

To investigate the structural determinants of binding, we determined the PDZ3 domain structure in complex with the PBMs of the four partners: myosin 15a, harmonin a1, CASK and taperin by X-ray crystallography. The crystal structures were solved by molecular replacement using the free form human PDZ3 from RIKEN Structural Genomics/Proteomics Initiative (RSGI) (PDB: 1UFX). Diffraction data collection and refinement statistics are summarized in Table S1. The overall RMSD of the backbone of PDZ3 between the free form (PDB: 1UFX) and the complexed forms are between 0.92 Å to 1.03 Å, which showed an equivalent overall backbone fold (Fig. 2).

1
2
3
4
5
6
7
8
9
10
11
12
13
14
15
16
17
18
19
20
21
22
23
24
25
26
27
28
29
30
31
32
33
34
35
36
37
38
39
40
41
42
43
44
45
46
47
48
49
50
51
52
53
54
55
56
57
58
59
60
61
62
63
64
65

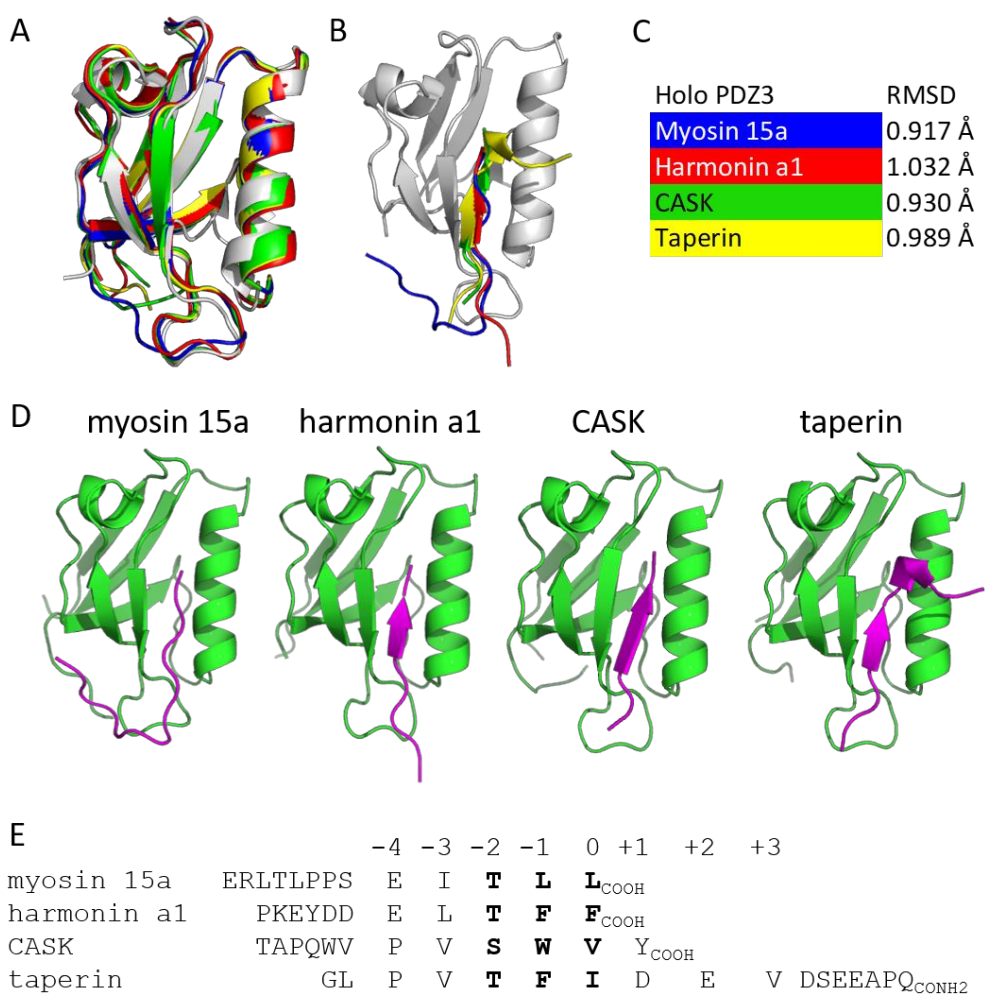


Figure 2: A: Backbone superimposition of 4 complexed PDZ3 and free PDZ3 (PDB: 1UFX), blue: myosin 15a, red: harmonin a1, green: CASK, yellow: taperin, white: free PDZ3. B : peptides superimposition with same colour set on the binding groove of apo PDZ3. C: overall RMSD values of PDZ3 backbone between free PDZ3 (PDB: 1UFX) and complexed PDZ3s. D: Crystal structures of PDZ3 in complex with PBMs from the four partners, myosin 15a, harmonin a1, CASK, and taperin with the PDB codes 6Y9N, 6Y9P, 6Y9O, 6Y9Q, respectively. E: Peptide sequence of each PBM, with position 0 corresponding to the residue forming H-bonds with ‘TLGI’ loop.

Structure and dynamics of the PDZ3/myosin 15a-PBM complex

Crystal structures of PDZ3ΔPBM, PDZ3/myosin 15a-PBM

As for the affinity determination, we have compared the structures of PDZ3 with and without the intramolecular PBM in complex with the myosin 15a PBM peptide (NH₂ERLTLPPSEITLL_{COOH}). The crystal structures of PDZ3/myosin 15a and PDZ3ΔPBM/myosin 15a were solved at 2.0 Å and 1.7 Å resolution, respectively, and are

1 very similar. The asymmetric unit of the PDZ3/myosin 15a crystal contains one
2 monomer, while PDZ3 Δ PBM/myosin 15a is a dimer, where myosin 15a peptides form
3 bridges tethering the two complexes (Fig. S1). As expected, PDZ3 of whirlin adopts a
4 typical PDZ fold comprising five β strands and two α helices and the peptide is inserted
5 into the PDZ-binding pocket through an interaction network specific to class I PDZ
6 domains that recognize the consensus peptide sequence $X-(S/T)-X-\Phi_{COOH}$, where X is any
7 residue (position -1), and Φ is a hydrophobic residue (position 0). The last residue
8 Leu(0) side chain is inserted in the hydrophobic core and the C-terminal carboxyl
9 oxygen forms H-bonds with Gly(826) and Ile(827) amide nitrogens from the 'TLGI' loop,
10 the 'GLGF' loop of whirlin. However, Leu(825) of 'TLGI' loop does not directly contact to
11 the terminus carboxylate of myosin 15a, that contrasts with PDZ/PBM structures
12 previously reported (Fig.3). Notably, a water molecule forms two H-bonds between
13 Leu(825) and one carboxylate oxygen atom. The side chain of Leu(-1) of myosin 15a
14 peptide is facing out, toward the hydrophobic side chain of Ala(828) on the PDZ β 2-
15 strand, that also contacts the side chain of Ile(-3). The three residues Leu(-1), Ile(-3) and
16 Ala(828) compose with the Val(843) side chain from the β 3-strand a hydrophobic patch
17 exposed at the surface of the intermolecular β -strand of complexed PDZ3. Thr(-2) forms
18 an H-bond with the His(876) side chain on α 2-helix as previously reported for a typical
19 Class I of PBM binding [22]. In addition, the residue Glu(-4) side chain carboxyl group
20 forms H-bonds with the Lys(877) side chain on α 2-helix, most likely contributing to the
21 high affinity of binding [37] (Fig. 3A3). Lys(877), found in mouse gene, is replaced by an
22 Arg in other species from zebra fish, *xenopus laevis* to mammals like horse, bovin, rat
23 and human. This substitution could establish a stronger double-bond with the Glu(-4)
24 side-chain of myosin 15a (Fig. S2).

25 In both PDZ3/myosin 15a and PDZ3 Δ PBM/myosin 15a structures, all the 13 residues of
26 the myosin 15a peptide are visible in electron density maps, and the last 5 residues
27 inserted in the binding groove attached to the β 2-strand fully overlay (Fig. 3A4).
28 However, the N-terminal of the myosin 15a peptide forms H-bonds with β 2 β 3 loop,
29 while in the crystal of PDZ3 Δ PBM/myosin 15a, such contacts were not observed.
30 Instead, the myosin 15a peptide binds to another PDZ3 domain organizing a dimer in
31 the crystal (Fig. S1). We concluded that the structural data on binding modes are
32 consistent with the affinity determination, and the PBM of whirlin does not affect the
33 binding of myosin 15a peptide to the PDZ3 domain.

34 *PDZ3 Δ PBM construct of whirlin is monomeric in solution*

35 The PDZ3 Δ PBM/myosin 15a complex formed a crystallographic dimer. In order to know
36 the oligomeric state of the complex in solution, we performed biophysical tests on the
37 purified PDZ3 Δ PBM domain. To estimate the oligomeric state of the PDZ3 Δ PBM domain,
38 Analytical Ultracentrifugation (AUC) and SAXS experiments were achieved with the
39 PDZ3 Δ PBM domain in free form and in complex with the PBM peptide of the myosin 15a
40
41
42
43
44
45
46
47
48
49
50
51
52

1 protein. Only one species of PDZ3 Δ PBM was detected for both free state or complexed,
 2 with a similar sedimentation coefficient of 1.21 S for the free form and 1.25 S for the
 3 complexed form. Both constructs show a frictional ratio of 1.4. showing similar shape
 4 with an onset of elongation. Taken together, these data are relatively consistent with a
 5 monomeric protein of 11kDa and a one to one complex of 12.6kDa, for the free and
 6 complexed PDZ3 Δ PBM, respectively. In agreement with the AUC experiments, we found
 7 by SAXS that the free and complexed PDZ3 Δ PBM behaves as a mono-disperse
 8 distribution of monomers in solution (Table 3). The estimated molecular mass of free
 9 and complexed PDZ3 derived from the extrapolated intensity $I(0)$ at the origin is
 10 consistent with the theoretical value of 11.3 kDa. In conclusion, both techniques showed
 11 that the PDZ3 Δ PBM in buffer (Tris 50mM, NaCl 150mM and TCEP 0.5mM) is on
 12 monomeric state in free and bound forms. This predominant monomeric state of PDZ3
 13 in solution was also observed by measuring its rotational correlation time (τ_c) by NMR
 14 experiments. The ^{15}N relaxation parameters T_1 , T_2 were determined for PDZ3 Δ PBM in
 15 apo form and in complex with myosin 15a. The τ_c values, estimated from the average
 16 T_1/T_2 ratio of non-flexible residues, are 6.1 and 7.3 ns for free PDZ3 Δ PBM and the
 17 PDZ3 Δ PBM /myosin 15a complex, respectively. In the free form, this value is in good
 18 agreement with the theoretical value of 5.4 ns expected for a 11.0 kDa globular domain
 19 (18.2 Å Stokes radius) (Table 3). We conclude that the PDZ3/myosin 15a and
 20 PDZ3 Δ PBM/myosin 15a complexes are monomeric in solution and have a 1:1
 21 stoichiometry in our NMR, SAXS and AUC experiments.
 22
 23
 24
 25
 26
 27
 28
 29
 30
 31
 32
 33
 34
 35
 36
 37

38 Table 3: Oligomeric state of PDZ3 monitored by SAXS, AUC and NMR rotational
 39 correlation time measurements.

	Rg (Å)	Dmax (Å)	Sedimentation coefficient (S)	τ_c (ns)
PDZ3 Δ PBM	15.18	66.94	1.21	6.1
PDZ3 Δ PBM+myosin15a	15.87	65.25	1.25	7.3

44
 45
 46
 47 *Dynamics in solution of PDZ3 Δ PBM in free form and in complex with myosin 15a PBM*

48 We have assigned the backbone NMR signals of PDZ3 Δ PBM. Over the 99 expected non-
 49 proline residues, 115 amide signals were visible in the HSQC spectrum and 95 backbone
 50 amide peaks could be assigned (96.0%). Backbone dynamics of PDZ3 Δ PBM in apo form
 51 and in complex with myosin 15a has been evaluated by measuring ^{15}N relaxation
 52 parameters (T_1 , T_2 and $\{^1\text{H}\}-^{15}\text{N}$ heteronuclear NOE). The ^{15}N relaxation parameters
 53 were analysed in terms of internal dynamic parameters (order parameter S^2 , internal
 54 correlation time τ_i and exchange parameter R_{ex}) using the Lipari-Szabo model-free
 55 approach (Fig. S5) [38]. Overall, the data showed a quite rigid PDZ domain in both free
 56
 57
 58
 59
 60
 61
 62
 63
 64
 65

1 and complexed states. Within each form, increased flexibility on the fast timescale (ps to
2 ns) is observed in the N- and C-terminus ends (residues 802-813, 902-903, respectively)
3 and in the loop connecting $\alpha 2$ - $\beta 5$ (891-894). In the complexed form, loops of PDZ3 are
4 globally more rigid (slightly higher S^2 values for residues 834-839, 858-860, 867-868,
5 890-892) on the fast timescale.
6

7 Interestingly, in the presence of myosin 15a partner, conformational exchange on the
8 microsecond to millisecond time-scale has been detected by shorter T_2 values in the
9 region around the binding site encompassing the $\beta 2$ - $\beta 3$ loop (residues 830-832; 837)
10 and the helix $\alpha 2$ (residues 877-887), that are in direct contact with the ligand, while the
11 end of helix $\alpha 1$ (852-856) is more rigid.
12
13
14

15 16 17 **Structure of the PDZ3/harmonin a1-PBM complex**

18 The crystal structure of PDZ3/harmonin a1 ($\text{NH}_2\text{PKEYDDELTFFCOOH}$) was solved at 3.2 Å
19 resolution with 6 copies in the asymmetric unit. Depending on the monomer, between 5
20 and 11 amino acids are observed in the electronic density. The C-terminal -TFF_{COOH}
21 sequence is a Class I PBM as the one of myosin 15a. The peptide inserted in a same way
22 as myosin 15a peptide in the PDZ binding groove. Notably, the Phe and Leu side chains
23 at positions -1 and -3, respectively, are facing outwards of the binding groove, and form
24 similar hydrophobic interactions with Ala(828) and Val(843) of the β -strand. We noted
25 that the proximity of the benzyl group from Phe(-3) triggers a strong chemical shift
26 perturbation (CSP) of the NH group from Ala(828) as monitored by NMR in solution
27 (Fig. S3). The peptide C-terminal carboxylate can only form weak H-bonds with the
28 'TLGI' loop (Fig.3B2). In addition, 3 out of 6 copies in the asymmetric unit have
29 deformed $\alpha 1$ helix, and in these 3 complexes (Fig.3B4), 1 of them formed H-bonds with
30 harmonin a1 carboxyl oxygen via its hydroxy oxygen of Thr of 'TLGI' loop. Meanwhile,
31 the positions -3 and -4 are conserved with hydrophobic and anionic residues,
32 respectively, -EI- for myosin 15a and -EL- for harmonin a1 sequences. However, we
33 observed no electron density for Glu(-4) in harmonin a1 and Lys(877) on $\alpha 2$ -helix that
34 reflects the flexibility of these side-chains. Thus, the absence of stable salt bridges
35 between these residues could explain the lower binding affinity of PDZ3 for harmonin a1
36 peptide than the one for myosin 15a.
37
38
39
40
41
42
43
44
45
46
47
48
49
50
51
52
53
54
55
56
57
58
59
60
61
62
63
64
65

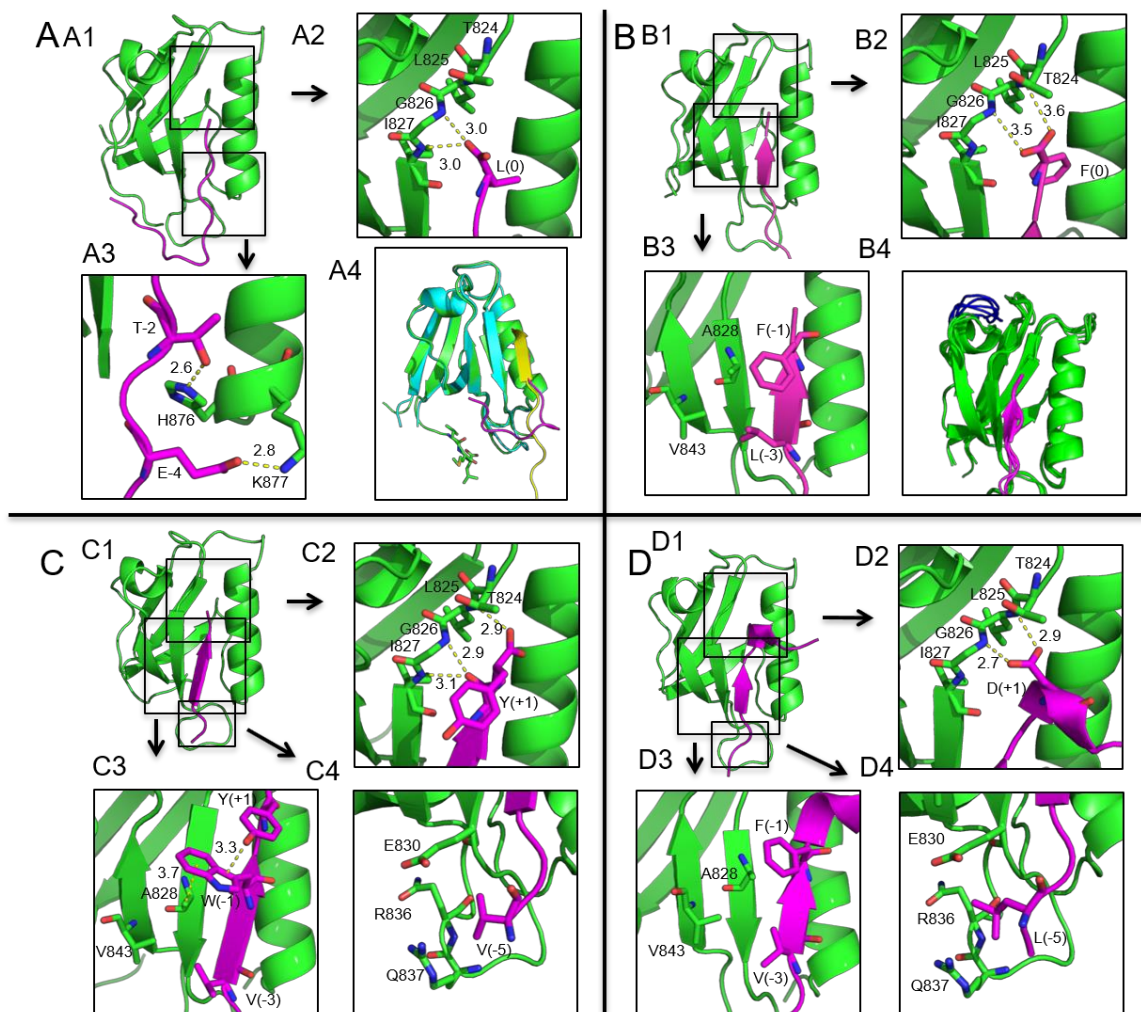


Figure 3: Binding details of four PDZ3-PBM peptide structures. Only hydrogen bonds distance lower than 3.7 Å are represented. A. PDZ3-myosin 15a. A2. Detailed the accommodation of PBM at 'TLGI' loop. A3. An extra side-chain interaction between Glu(-4) of myosin 15a and Lys(877). A4. An overlay view of PDZ3/PDZ3ΔPBM-myosin 15a, where last three residues -VML are in stick-shape. PDZ3ΔPBM-myosin 15a complex are in colour cyan and yellow. B. PDZ3-harmonin a1. B2. Detailed the 'TLGI' loop with PBM. B3. Phe(-1) and Leu(-3) of harmonin a1 at the hydrophobic surface of β2- and β3-strands. B4. Overlay of all six copies in the asymmetric unit, where three of them have the deformation of α-helix 1 coloured in blue. C. PDZ3-CASK. C2. Detailed the 'TLGI' loop with peptide C-terminus. C3. π-π offset packing between Tyr (1) and Trp(-1). Hydrophobic stacking of Trp(-1) and Val(-3) at the surface of β2- and β3-strands. C4. Val(-5) at the pocket formed with Glu(830), Arg(836) and Gln(837) aliphatic side-chains. D. PDZ3-taperin. D2. Side-chain of Asp1 mimics C-terminus PBM carboxylate group, forming 2 H-bonds with 'TLGI' loop. D3. Phe(-1) and Val(-3) of taperin at the surface of β2 and β3-strands. D4. Hydrophobic contacts between Leu(-5) and a pocket formed by Glu(830), Arg(836) and Gln(837) aliphatic side-chains.

Structure of the PDZ3/CASK-PBM complex

The crystal of PDZ3 complexed to the internal PBM of CASK ($\text{NH}_2\text{TAPQWVPVSWVYCOOH}$) diffracted at 1.6 Å resolution. The asymmetric unit only contains one copy of the complex, and the last 7 residues -VPVSWVY COOH are well defined in the electron density. In this structure, PDZ3 still recognized a Class I -SWV- as a PBM shifted by one position. The amide oxygen of Val(0) is located at the same position as the myosin 15a and harmonin a1's carboxyl oxygen; the side chains of CASK-Val(0), harmonin a1-Phe(0) and myosin 15a-Leu(0) perfectly superimpose, pointing toward the PDZ pocket. The Val(0) carbonyl oxygen and the Tyr(+1) carboxyl oxygen form three H-bonds, mimicking the C-terminus carboxyl group on 'TLGI' loop (Fig. 3C2). The Trp(-1) side chain is facing out of the binding groove towards the hydrophobic surface of the $\beta 2$ and $\beta 3$ -strands. Interestingly, the indole side chain is packed to the Tyr(+1) side chain to form a π - π offset packing, where the Tyr side chain hydroxyl group is 3.3 Å away from the indole group of Trp (Fig. 3C3). This aromatic packing seems to be very important for the backbone and side-chain orientations of CASK peptide in the binding groove to satisfy the network of hydrogen bonds with PDZ3. Ser(-2) is positioned in a reminiscent way of Thr(-2) of myosin 15a and harmonin a1, and forms the classical H-bond with His side chain on the $\alpha 2$ -helix. The Pro(-5) side chain of CASK peptide is located near the side chain of His on $\alpha 2$ -helix, creating potential CH- π interaction [39], and the Pro(-5) C γ is 3.8 Å away from the His(876). The Val(-6) side chain points toward the aliphatic side chain of Arg(836) from the $\beta 2$ - $\beta 3$ loop (Fig. 3C4).

Structure of the PDZ3/taperin-PBM complex

The crystal structure of the complex formed by PDZ3 and the internal ($\text{NH}_2\text{GLPVTFIDEVDSEEAPQCONH}_2$) peptide of taperin was solved at 1.3 Å resolution. The N-terminal 11 residues, -GLPVTFIDEVD-, are well ordered in the crystal (Fig. 3D). PDZ3 recognises the internal PBM of taperin peptide (-TFI-) as a class I PBM. Thr(-2) forms a H-bond with His imidazole nitrogen on PDZ3 $\alpha 2$ -helix as a classical class I PDZ interaction motif. The Phe(-1) side chain is closed to the hydrophobic surface of $\beta 3$ -strand and facing outside the binding groove in a similar position to the one adopted by Phe(-1) of the harmonin a1 peptide with only a slight shift of the phenyl group by 1.6 Å. Ile(0) has its side chain pointing towards the binding groove with its hydrophobic side chain as observed for typical last residue of C-terminal PBM. Ile(0) however participated to the formation of a short α -helix of three residues encompassing the two downstream residues Asp(+1) and Glu(+2). Interestingly, side chain carboxyl group of Asp(+1) turns back and forms H-bonds with the backbone amide of Leu and Gly with 'TLGI' loop, and consequently mimics the C-terminal PBM hydroxyl binding similar to the harmonin a1 peptides but stronger H-bonds (Fig. 3D2). In the short helix of taperin peptide, Ile(0)

1 with Glu(+2) and Asp(+1) with Val(+3) formed two intramolecular H-bonds to maintain
2 the helical conformation. In this structure, the Pro(-4) side chain positioned as a 90°
3 vertical to the side chain of His on α 2-helix, at the same location and same position as
4 the Pro in the PDZ/CASK-PBM complex. Moreover, as also observed in the PDZ/CASK-
5 PBM complex, the Leu(-5) side chain is stabilized by hydrophobic contacts involving the
6 aliphatic side chains of Arg(836) in the β 2- β 3 loop and of Glu(830) from the β 2-strand
7 (Fig. 3D4).
8

9
10 Interestingly, the two internal motifs of CASK and taperin have sequences close to
11 the consensus peptide; Φ -P- Φ -S/T - Ω - Φ (position 0)-, where Φ is a hydrophobic residue,
12 and Ω is an aromatic residue, which is similar as predicted whirlin internal PBM binding
13 pattern -T-[FLV]-I- previously reported by yeast two hybrid screening [40]. As a
14 consequence, we noted that the N-terminals part of taperin-PBM and CASK-PBM,
15 encompassing the hydrophobic position -5, Leu and Val, respectively, are in close
16 contact with the β 2- β 3 loop and well superimposed while a shift between 2.4 and 3.2 Å
17 of this loop toward the binding groove is observed for PDZ3 in complex with the two
18 canonical PBMs from myosin 15a and harmonin a1.
19
20
21
22
23
24
25
26
27
28
29
30
31
32
33
34
35
36
37
38
39
40
41
42
43
44
45
46
47
48
49
50
51
52
53
54
55
56
57
58
59
60
61
62
63
64
65

Discussion

1 Proteins encoded by *Usher* genes contain numerous scaffolding domains and protein-
2 protein interaction motifs necessary to the intricacy of the molecular networks in hair
3 cells. Remarkably, out of the nine Usher proteins involved in the development of
4 stereocilia and the mechano-transduction machinery, eight possess short C-terminal
5 PBM motifs, but only 2 Usher proteins have PDZ domains – whirlin and harmonin.
6 Through their PDZ domains, as well as other scaffolding domains, these two paralogous
7 proteins are qualified to assemble transient multi-protein complexes that coordinate the
8 development of stereocilia as well as the mechano-transduction signalling. PDZ domains
9 are dynamic tools for PPI, suited for multi-target binding environment. As illustrated by
10 our results with the PDZ3 of whirlin, PDZ domains interact with their PBM-containing
11 partners mainly with short residence time resulting in weak to medium binding
12 affinities (1-100 μM). In the hair cells, whirlin controls the stereocilia elongation and the
13 planar polarity during development and also participates in the mechano-transduction
14 signalling, stereocilia bundle cohesion and neuronal connection at the ribbon synapse
15 [7][41][10][42][16]. In photoreceptors, whirlin is involved in the renewal of the light-
16 sensitive receptor protein rhodopsin, while it is also involved in the mechanosensory
17 signalling of proprioceptors [43]. This pleiotropic function of whirlin relies on its
18 capacity to participate in various protein complexes. Whirlin is found at different
19 locations in the hair cells, such as at the tip, ankle links and synapse, with many different
20 isoforms whose expressions are regulated in time and space. As illustrated by *in vitro*
21 investigations, the PDZ1 domains of whirlin and harmonin are multi-PBM binders, by
22 contrast with their second PDZ domain [12].

23 Here, we report that the PDZ3 domain of whirlin, present in both the full-length
24 and short C-terminal isoforms expressed in hair and photoreceptors cells, is also a multi-
25 partner binder, thanks to its unique capacity to accommodate non-canonical binding
26 motifs. By contrast with the two N-terminal PDZ domains of whirlin involved in
27 heterotypic and homotypic supramodule [12], we showed that its PDZ3 is fully
28 independent from other domains at the C-terminal end of the protein, facilitating its
29 accessibility to potential ligands. We quantified for the first time the *in vitro* interactions
30 between the last PDZ domain of whirlin and all PBM-containing peptides from Usher
31 proteins using the high-throughput *Holdup* chromatographic assay and SPR. Four Usher
32 binders have been identified, myosin 15a and cadherin 23 with high affinity of few μM ,
33 harmonin a1 with a moderate affinity 20 to 40-fold lower, and protocadherin 15 CD3
34 with a low affinity (250 μM). In addition, non-Usher binders have been pinpointed;
35 CASK, a well-known neuronal kinase, and taperin, a known deafness protein, which
36 respectively interact with moderate to high affinity. Interestingly, these two partners
37 possess internal PDZ binding motifs that efficiently recognize whirlin. By deeply
38 characterising the dynamical and structural properties of the PDZ3 domain of whirlin in
39
40
41
42
43
44
45
46
47
48
49
50
51
52
53
54
55
56
57
58
59
60
61
62
63
64
65

1 this work, we identified some features that could contribute to the promiscuity of the
2 domain. We solved the four high-resolution structures of the binders myosin 15a,
3 harmonin a1, taperin and CASK complexed to whirlin PDZ3. These proteins have been
4 reported to interact or co-localize with whirlin in hair cells or photoreceptor cells [14]
5 [18][24][25][26] [21][20].
6

7 The four PDZ/ligand complexes, comprising two C-terminal (myosin 15a and
8 harmonin a1) and two internal motifs (CASK and taperin), adopt a class I network of
9 interactions; with their hydrophobic residue at position 0 inserted in a dedicated pocket
10 of the PDZ and their Thr/Ser (-2) interacting with the conserved His on the PDZ $\alpha 2$ helix
11 [22]. Interestingly, the PDZ3 domain is very permissive concerning the network of
12 hydrogen bonds between the residue at position 0 and the 'TLGI' loop, as well as the
13 recognition of the PBM at position -1, which could result from two distinct structural
14 features. (A simplified LigPlot version is in supplementary Fig. S6)
15
16

17 First, whirlin PDZ3 possesses a singular long $\alpha 2$ -helix (13 residues) in
18 comparison with the PDZ1 and PDZ2 domains (7 and 8 amino acids long, respectively),
19 resulting in between one to two supplementary C-terminal helical turns. Among the six
20 PDZ domains encoded by Usher proteins, this longer $\alpha 2$ -helix is also observed in the
21 PDZ3 of harmonin and PDZD7 (Fig. S4). Interestingly, Phe(887) in the last C-terminal
22 turn of $\alpha 2$ -helix is facing the binding groove. The orientation of the Phe side chain is
23 constrained by hydrophobic contacts with Lys(820), Leu(825) and Ile(895) on the 'TLGI'
24 loop and the $\alpha 2$ - $\beta 5$ loop. One consequence of this side-chain orientation is the shift of
25 the 'TLGI' loop away from the binding groove due to steric hindrance. The aliphatic core
26 of Lys(820) on the upstream 'TLGI' loop and the aromatic group of Phe form a strong
27 antiparallel lock to stabilize the conformation of both loops and the $\alpha 2$ -helix. In addition,
28 Lys(820) further stabilizes the extra-long $\alpha 2$ -helix by forming three H-bonds with the
29 backbone carbonyl oxygens of the $\alpha 2$ -helix and the $\alpha 2$ - $\beta 5$ loop. Interestingly, Thr(889)
30 has its backbone carbonyl oxygen facing towards amine group of Lys(820) with a C-N-O
31 angle nearly 180° and only 2.8 Å away from each other. This network of hydrogen bonds
32 involving the lysine NH_3^+ group and backbone carbonyl has been documented before for
33 its role in capping the C-terminus of α -helices [44]. This original conformation of the top
34 of the binding groove is observed in our four complexes structures but also in the
35 absence of ligand, in the NMR structure of the free PDZ3 (PDB: 1UFX). This 'Lys-Phe
36 lock' is strictly conserved in all orthologous whirlin sequences, the Phe being substituted
37 by a Trp in harmonin and a Tyr in PDZD7 (Fig. S4). This lock features found in all four
38 complexes most likely increase the rigidity of the upper part of the binding groove in
39 agreement with our NMR dynamics measurements (Fig. 4, S5). We propose that this
40 stable structure of the extra-long $\alpha 2$ -helix facilitates the protein-protein interaction with
41 a greater diversity of binders. The upper part of the binding groove is more constrained
42
43
44
45
46
47
48
49
50
51
52
53
54
55
56
57
58
59
60
61
62
63
64
65

and is entropically favourable to accommodate non-canonical peptide such as the internal PBM of taperin.

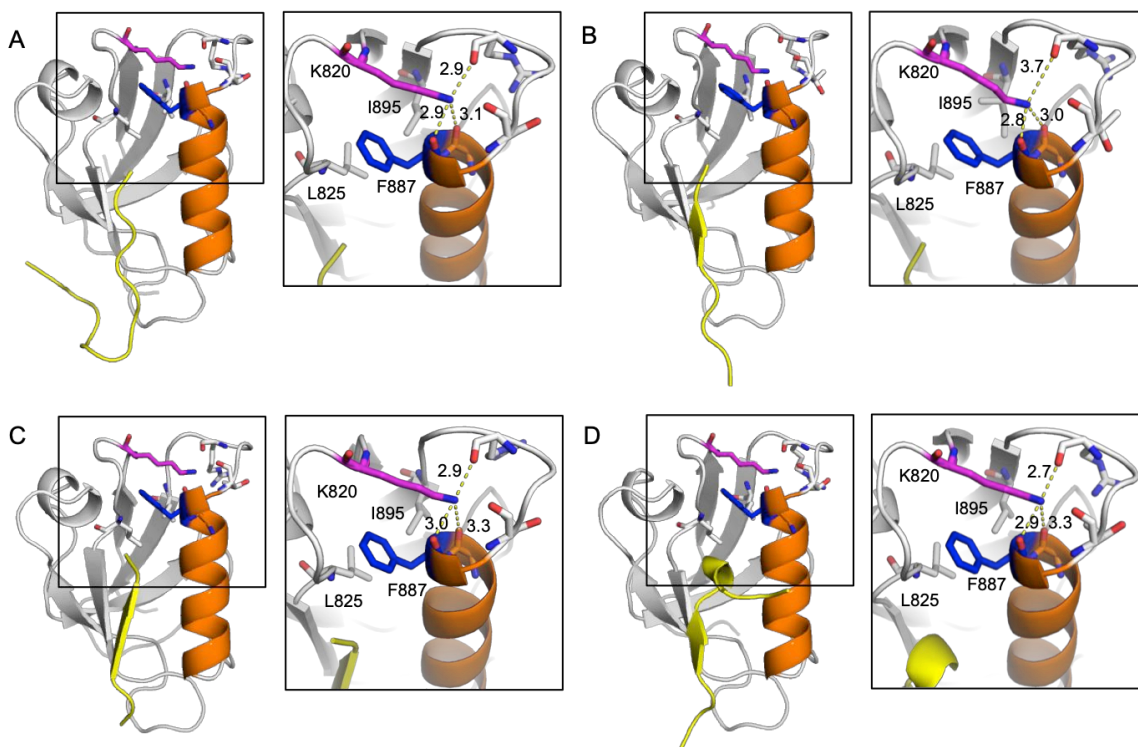


Figure 4: the 'Lys-Phe lock' at the top of 'TLGI' loop and $\alpha 2$ -helix in the four PDZ-PBM complexes. A. PDZ3/myosin 15a. B. PDZ3/harmonin a1. C. PDZ3/CASK. D. PDZ3/taperin. Yellow: the peptide. Orange: the $\alpha 2$ -helix. Magenta: Lys820. Blue: Phe887. Distances are shown by dash lines with threshold 3.8 Å.

The slightly far-away Leu on the 'TLGI' loop extended the upper part of the PDZ3 binding pocket, thus suitable for internal PBM recognition (Fig. 3). In the case of the canonical PBM of myosin 15a, only one H-bond is formed between this 'TLGI' loop and the COOH of PBM, which is unique for PDZ-PBM binding. However, in the non-canonical binding CASK and taperin PBM, the 'TLGI' loop forms two H-bonds respectively. In addition, the carboxyl side-chain at position +1 of taperin internal PBM curves back and mimics the C-terminus carboxyl group (Fig. 3D2). The PBM of CASK, shifted by a single residue, which has never been reported before, in which the final residue Tyr is exposed to the solvent together with the Trp at position -2, forms a π - π offset, a well-documented type of interaction [45][46][47], that contributes to the stability and function of biomolecules. Samanta and coworkers mentioned that the π - π stacking of Tyr and Trp appears as an edge stacking like the OH- π interactions, as exhibited in the CASK structure [48].

1
2
3
4
5
6
7
8
9
10
11
12
13
14
15
16
17
18
19
20
21
22
23
24
25
26
27
28
29
30
31
32
33
34
35
36
37
38
39
40
41
42
43
44
45
46
47
48
49
50
51
52
53
54
55
56
57
58
59
60
61
62
63
64
65

Second, the exposed and flat hydrophobic surface of the β 2-strand also facilitates the ligand accommodation, which could explain part of the versatility of PDZ3 to bind various PBMs. The β 2 strand is formed by 4 residues: Ile-Ala-Ile-Glu. The small hydrophobic side chain of Ala(828) is exposed onto the surface with potential interactions with the positions (0) to (-2) of the PBM peptide. Thus, this hydrophobic surface makes it possible for the large hydrophobic (Leu) or aromatic residues (Phe or Trp) to adapt at these positions, as observed for the PBM sequences of all the four partners we studied (Fig.3). Val(843) from the β 3-strand of PDZ3 fill-up the hydrophobic patch exposed at the surface of the β -strand and also participates to the PBM binding, mainly with the conserved position -3 of all four partners, which is systematically a hydrophobic residue, Leu or Val.

In this study, we showed that the PDZ3 of whirlin interacts with myosin 15a, harmonin a1, CASK and taperin PBM via either canonical or non-canonical PDZ-PBM binding, but also with cadherin 23 and protocadherin15-CD3. This variety of ligands likely reflects the different functions of whirlin in its various environments in hair cells and photoreceptors. Whirlin fulfils a function of scaffolding, participating in different complexes along the stereocilia. During the stereocilia development, it is well documented that whirlin localizes at the transient ankle links at the root region and at the tips of the tallest stereocilia row [16]. At the tip, whirlin has been previously reported to co-localize and interact with actin motor protein myosin 15a, two related MAGUK family proteins CASK and MPP1, GPSM2, and the actin regulation protein EPS8. The myosin 15a is a well-known binding partner of whirlin. It helps transporting whirlin to the tip of stereocilia, and remains in the protein complexes at the tip [14]. Altogether, these proteins play a crucial role in the regulation of actin dynamics according to their localization along the stereocilia. At ankle region of stereocilia, the scaffolding whirlin is proposed to adopt a polar organization in the cytoplasm, where its N-terminus is facing the cell membrane to form the USH2 complex with PDZD7, Usherin and ADGRV1, mainly through PDZ/PBM interactions [49], while the C-terminus is in contact with the actin filaments, potentially by the interaction with actin-binding protein such as myosin 7a even though the implication of PDZ3 is unclear in this process. The non-syndromic deafness DFNB79 related protein taperin is also expressed at the base of the stereocilia and its depletion affects the length and orientation of stereocilia and eventually causes stereocilia loss [34][35][36]. Taperin is also reported interacting with GRXCR2 (Glutaredoxin domain-containing cysteine-rich protein 2) in the taper region. In the GRXCR2 knockout mice, the taperin has two main distinct localizations in the early development stage: at the base and tip of stereocilia, exactly where whirlin localizes [50]. Here, we identified the interaction between taperin and whirlin *in vitro*, and we propose a potential interplay between the taperin/GRXCR2 and USH2 complexes at the basal region of stereocilia.

1 The C-terminal region of whirlin coding for its third PDZ domain undoubtedly
2 participates to the interactions with others proteins in the ankle link complex, with
3 USH1 proteins forming USH1/USH2 complexes, as already observed with SANS and
4 myosin 15a in photoreceptors, and potentially with cadherin 23 and protocadherin 15-
5 CD3 along the stereocilia, but also with other deafness proteins such as taperin or
6 catalytic protein such as CASK. Further studies are needed to unravel these different
7 interactions in the development and functioning of sensorial cells.
8
9

10 11 12 **METHODS**

13 **Constructs cloning, expression and purification**

14 The constructs used: HHD2 (420-499), Proline-rich (PR) region (500-808), PDZ3ΔPBM
15 (809-903), PDZ3 (809-906), HHD2-PR (420-808), PR-PDZ3 (500-906). The constructs of
16 whirlin were synthesized from cDNA of *Mus musculus* whrn isoform 4 (UniprotKB
17 number Q80VW5-4). Constructs HHD2, PDZ3ΔPBM and PDZ3 were subcloned into a
18 pGST//2 expression vector (derived from pGEX-4T-1; Amersham) with an ampicillin
19 resistant cassette. Constructs PR, HHD2-PR and PR-PDZ3 were subcloned pHTP1 vector
20 by commercial kit: NZYEasy Cloning kit at NZYtech company. A TEV protease cleavage
21 site was introduced between the N-terminal GST or His tag and the protein sequence.
22

23 The constructs plasmids were transformed into *E. coli* BL21 (DE3) star (Invitrogen)
24 strain. Bacteria were grown in LB or isotope (¹⁵NH₄Cl and/or ¹³C-glucose) labelled M9
25 minimal media at 37°C. The expression was induced by 1mM IPTG (Isopropyl β-D-1-
26 thiogalactopyranoside) at OD_{600nm} 0.8 to 1.0, at 30°C for 3 hours. Bacteria were then
27 harvested and resuspended in lysis buffer (Tris pH 7.5 50mM, NaCl 250mM, β-
28 mercaptoethanol 2mM and protease inhibitor 1 table per 50ml (Complete, EDTA-free,
29 Roche Diagnostics)). Then, the cells were broken by sonication, and the debris were
30 pelleted by centrifugation (30,000g, 1 h, 4°C). The GST tag fused proteins were purified
31 by affinity chromatographies column: GSTrap HP (GE Healthcare) or nickel chelated
32 HiTrap Chelating HP (GE Healthcare), followed by a TEV protease cleavage at 4°C
33 overnight. Then, the next day, a final step of a size-exclusion chromatography (SEC) was
34 achieved by using Sephacryl S-100 HR 16/600 (GE Healthcare) with buffer Tris pH 7.5
35 50mM, NaCl 150mM, TCEP 0.5mM.
36
37

38 **Holdup assay with human PDZ domains**

39 The peptides were synthesized in solid phase using Fmoc strategy (Proteogenix)
40 encompassing a biotinyl group, a (PEG)₃ spacer and the C-terminal PBM sequence of
41 Usher proteins (11 to 16 residues long). All PDZ domains (244 to 259 over 266 PDZ
42 domains identified in the human genome) were expressed following the high-
43 throughput protocol previously described [27][51].
44

45 The holdup assay was carried out as previously described [27]. The minimal Binding
46 Intensity (BI) threshold value to define a significant interaction is 0.2.
47
48
49
50
51
52
53
54
55
56
57
58
59
60
61
62
63
64
65

SPR experiments

Interactions between whirlin and Usher peptides were characterized by SPR using a ProteOn XPR 36 system (Biorad) equilibrated with a buffer containing NaCl 250mM, Tris pH 7.5 50mM, TCEP 0.5mM. Biotinylated peptides were captured as ligands on a Neutravidin-functionalized NLC sensor chip (Biorad), over which the different whirlin fragments were flowed as analytes at 20 μ L/min for 2 minutes. The steady-state SPR responses (R_{eq} , experimental or extrapolated) were plotted against the concentration (C) of analyte and fitted using the following equation, $R_{eq} = (R_{max} * C)/(K_d + C)$, where K_d is the equilibrium dissociation constant, and R_{max} the maximal binding capacity of the surface, using BIAevaluation 4.1 software (Biacore).

Phage display

Protein purification for phage display

His-MBP-tagged whirlin PDZ3 fusion protein was expressed in *E. coli* BL21-gold (DE3) in 2YT media (1.6 % (w/v) tryptone, 0.5 % NaCl, 1 % yeast extract) supplemented with carbenicillin (100 μ g/ml). Bacteria were pelleted by centrifugation and incubated at -20°C 1h before lysis with Bacterial Cell Lysis Buffer (NZYtech). The protein was purified by affinity chromatography using Ni-sepharose beads and eluted with 300 mM imidazole.

ProP-PD selections

ProP-PD selections were carried out following a published protocol [33] with few alterations. The MBP-tagged PDZ domain (30 μ g in 100 μ l PBS) was immobilized in a MaxiSorp flat-bottom 96-well plate (Nunc). For the use in pre-selection, 200 μ l blocking solution (PBS with 0.5 % BSA) was immobilized in a different well. The proteins were immobilized overnight at 4°C, before the PDZ coated well was blocked with 200 μ l blocking solution. The wells were washed four times with 200 μ l PBS. An M13 phage library displaying 16 amino acid peptides covering the intrinsically disordered regions of the human proteome [33] was added to the pre-selection well for 1 h, before being transferred to the MBP-PDZ3 coated well. After 2 h incubation at 4°C, unbound phage particles were removed by four times washing with 200 μ l PT buffer (PBS, 0.05% (v/v) Tween-20), while bound phage particles were eluted with 100 μ l log-phase OMNImax™ *E. coli* (Thermo Fischer Scientific). After a 30 min incubation at 37°C, 10 μ l M13K07 helper phage (1x10¹¹ p.f.u./ml, New England Biolabs) were added and the culture was incubated at 37°C for another 45 min. Finally, the culture was added to a deep-well 96-well plate with 1.1 ml 2YT media supplemented with 100 μ g/ml carbenicillin, 30 μ g/ml kanamycin and 1 mM IPTG, which was incubated at 37°C overnight. The next day, the bacteria were spun down at 2,000 g and 800 μ l phage supernatant was transferred to a new well and incubated 10 min at 65°C to kill remaining bacteria. The phage solution

1 was chilled, and pH adjusted by the addition of 1/10 volume of 10 x PBS, before being
2 used in a new round of selection. Five rounds of selection were completed.

3 The phage supernatant from each selection day was analysed for enrichment of binding
4 phage by phage ELISA. MBP-PDZ3 (10 µg in 50 µl PBS) was immobilized in a MaxiSorp
5 plate and incubated overnight at 4°C. The MBP-PDZ3 coated well and a control well
6 were then blocked using the blocking solution. After 1 h incubation at 4°C, the wells
7 were washed four times with PT buffer, and then incubated 2 h with 50 µl phage pool
8 per well. Subsequently, the wells were washed four times with 200 µl PT buffer, before
9 100 µl horseradish peroxidase-conjugate anti-M13 antibody (BioSite) (1:5,000 dilution
10 in PT buffer with 0.5 % BSA) was added for a 1h incubation. The wells were washed five
11 times with 200 µl PT buffer. 50 µl of 1:1 mix of TMB (3,3',5,5'-Tetramethylbenzidine)
12 and peroxide solution (VWR) was added as HRP substrate. The reaction was stopped
13 using 50 µl 0.6 M H₂SO₄. The signal from both control and MBP-PDZ3 well was measured
14 spectrophotometrically at 450 nm. The ratio between the signal from the MBP-PDZ3 and
15 control well was calculated to evaluate the enrichment of binders over the days of
16 selection, and the peptide coding region from the binding enriched phage pools were
17 amplified and barcoded by PCR as described elsewhere [33] before being analysed by
18 next-generation sequencing on the Ion torrent platform.
19
20
21
22
23
24
25
26
27
28

29 **Small Angle X-ray Scattering (SAXS)**

30 X-ray scattering data were collected at the SWING beamline at Soleil synchrotron
31 (Saclay, France). 50µl of sample (protein concentration 9.75 g/l, the mixture has protein
32 and peptide 1:2 ratio) was injected on a Superdex-75 5/150GL (GE) size exclusion
33 column in-line with the SAXS measuring cell.
34

35 Frames with a duration of 1s were recorded during the whole elution time.
36
37 Approximately 100 frames recorded in the dead volume of the column were averaged to
38 generate the buffer subtraction curve and 10 to 30 frames corresponding to the top of
39 the elution peak were averaged to generate the result curve. Primary data reduction was
40 performed using the program FOXTROT (Xenocs SAS). The one-dimensional scattering
41 intensities are expressed as a function of the modulus of the scattering vector $Q =$
42 $4\pi\sin\theta/\lambda$ with 2θ being the scattering angle and λ the X-ray wavelength. Buffer
43 intensities were subsequently subtracted from the respective sample intensities using
44 the software package PRIMUS [52]. The radii of gyration were evaluated using Guinier
45 approximation [53]. Dmax was determined from distance distribution function P(r)
46 obtained with the program GNOM [54].
47
48
49
50
51
52
53
54
55

56 **Fluorescence measurements**

57 Measurements of fluorescence emission were performed at 25°C in a LS50
58 spectrofluorometer (PerkinElmer) using a 109F cuvette (Hellma Analytics). Excitation is
59 set at 295 nm to excite only Tryptophan and emission spectrum is recorded from 300
60
61
62
63
64
65

1 nm to 450 nm, with a 5 nm bandwidth for both. Peptide (CASK-PBM: TAPQWVPVSWVY)
2 was diluted in the buffer (Tris 50 mM pH 7.5, NaCl 150 mM, TCEP 0.5 mM) at
3 concentration 2.4 μ M. Buffer fluorescence is subtracted from peptide emission spectra
4 and the spectra were corrected according to the measured concentration. The titration
5 curve fitting was done with software Origin 7.5.
6
7
8

9 **Sedimentation velocity - Analytical Ultracentrifugation (AUC)**

10 Sedimentation velocity experiments were performed on an XL-I ultracentrifuge
11 (Beckman-Coulter, Brea, CA, USA). Oligomerization state of PDZ3 Δ PBM in presence and
12 absence of 0.6 mM myosin 15a peptide were determined. Samples at 4 mg/ml were
13 loaded in cells equipped with 1.2 cm double-sector epoxy centerpieces and sapphire
14 windows. Samples were equilibrated for 2h at 20°C in an 4-hole AN60-Ti rotor and then
15 spun at 42,000 rpm for 15h. Rayleigh interference profiles were recorded.
16 Sedimentation profiles were analyzed using the continuous size distribution model $c(s)$
17 of the software Sedfit [55]. All the $c(s)$ distributions were calculated with a fitted
18 frictional ratio f/f_0 and a maximum entropy regularization procedure with a confidence
19 level of 0.68. The protein partial specific volume of 0.740 ml/g was theoretically
20 determined with Sednterp. Samples were prepared in 50 mM TRIS, 50 mM NaCl pH 8
21 and buffer density and viscosity at 20°C of 1.005 g/ml and 1.016 cP, respectively, were
22 also calculated with Sednterp.
23
24
25
26
27
28
29
30
31

32 **NMR Spectroscopy**

33 All NMR experiments were performed at 25°C on a 600 MHz Bruker Avance III
34 spectrometer equipped with a TCI cryoprobe and analyzed with CcpNmr Analysis 2.4
35 software [56].
36
37

38 *Protein assignment.* The backbone $^1\text{H}^{\text{N}}$, ^{15}N , $^{13}\text{C}\alpha$, $^{13}\text{C}\beta$ and $^{13}\text{C}\text{O}$ resonance assignment of
39 PDZ3 Δ PBM was performed on a 0.8 mM $^{15}\text{N}/^{13}\text{C}$ -labeled sample (sodium phosphate, pH
40 6.5, 2mM TCEP and 150mM NaCl) using 2D ^1H - ^{15}N HSQC and the following BEST- or
41 BEST-TROSY-based 3D experiments: HNC0, HNC0+, HN(CA)CO, HN(CO)CACB, HNCACB.
42
43

44 *Protein dynamics.* The ^{15}N relaxation times (T_1 and T_2) and $\{^1\text{H}\}$ - ^{15}N heteronuclear NOE
45 were measured on a 0.2 mM ^{15}N -labeled sample of PDZ3 Δ PBM (Tris 50m, pH7.0,
46 150mM NaCl and 2mM TCEP) in the absence and presence of a 2-fold excess of myosin
47 15a peptide. Experiments were recorded by standard methods [57], in an interleaved
48 manner with a recycling time of 3 s and with 7 relaxation delays for T_1 (20, 100, 200,
49 400, 600, 800, 1200 ms) and 8 for T_2 (17, 34, 51, 68, 85, 119, 153, 238 ms). The
50 heteronuclear NOE were recorded in the presence and absence of a 3 s ^1H saturation
51 sequence (120° ^1H pulse train), with a recycling delay of 5 s. The relaxation parameters
52 were analyzed using the model-free formalism of Lipari and Szabo [38] with the
53 program TENSOR2 [58] to extract internal dynamical parameters (amplitude of the
54
55
56
57
58
59
60
61
62
63
64
65

1
2
3
4
5
6
7
8
9
10
11
12
13
14
15
16
17
18
19
20
21
22
23
24
25
26
27
28
29
30
31
32
33
34
35
36
37
38
39
40
41
42
43
44
45
46
47
48
49
50
51
52
53
54
55
56
57
58
59
60
61
62
63
64
65

picosecond to nanosecond time scale motion S^2 , internal correlation time τ_i and exchange parameter R_{ex}). An isotropic model, with a correlation time τ_c , was sufficient to describe the global reorientation of the protein and an anisotropic model did not improve the fit.

Peptide titration. PDZ3 (and PDZ3 Δ PBM) samples initially contained about 200 mM ¹⁵N-labeled PDZ3 in 300 μ L of buffer containing Tris 50mM, pH7.0, 150mM NaCl and 2mM TCEP. Unlabeled peptide was added stepwise to a final PDZ/peptide ratio of 1:4, 1:10 and 1:11 for myosin 15a, harmonin a1 and taperin peptides, respectively. ¹H-¹⁵N HSQC spectra were recorded at 13, 15 and 9 different titration points, respectively. For myosin 15a and harmonin a1, average (¹H, ¹⁵N) chemical shift changes were calculated as $\Delta\delta_{avg} = ((\Delta\delta H)^2 + (\Delta\delta N \times 0.159)^2)^{1/2}$. For taperin, the variations of the bound signal intensity were followed because of the slow exchange binding process with this peptide. The dissociation constants (Kd) of the respective complexes were obtained by fitting the titration data ($\Delta\delta_{avg}$ or intensities) with a model assuming a 1:1 complex formation and with nonlinear regression.

Crystallization and diffraction data collection

Crystallization screening trials were performed at the Crystallography Platform of the Institut Pasteur [59]. For the initial screenings, sitting drops of 400 nL (1:1 protein to precipitant ratio) were set up in 96-well Greiner plates with a Mosquito automated nanoliter dispensing system (TTP Labtech, Melbourn, UK). The plates were then stored in a RockImager (Formulatrix, Bedford, USA) automated imaging system to monitor crystal growth. Crystallization conditions corresponding to the different complexes between whirlin PDZ3 and peptides are detailed in Table S1. Diffraction data were collected at beamlines PROXIMA 1, PROXIMA 2a (SOLEIL synchrotron, St. Auban, France), and ID-29 (Synchrotron ESRF, Grenoble, France) and processed with XDS [60] and Aimless [61].

Structure determination and model refinement

The crystal structures of whirlin PDZ3 in complex with the different peptides were solved by the molecular replacement technique using the PDZ3 domain of the human KIAA1526 protein (PDB 1UFX) as search model with Phaser [62]. Final models of the complexes were obtained through interactive cycles of manual model building with Coot [63] and reciprocal space refinement with Buster [64] and phenix.refine [65]. X-ray diffraction data collection and model refinement statistics are summarized in Table S1. Figures showing the crystallographic models were generated with PyMol (Schrodinger, LLC, version 2.4.0a0).

Data and PDB code availability

Atomic coordinates for the whirlin PDZ3/PDZ3 Δ PBM in complexes with ligand PBMs have been deposited in the protein data bank with accession code 6Y38, 6Y9N, 6Y9O, 6Y9P and 6Y9Q. 6Y38: PDZ3 Δ PBM+myosin 15a peptide, 6Y9N: PDZ3+myosin 15a peptide, 6Y9O: PDZ3+CASK peptide, 6Y9P: PDZ3+harmonin a1 peptide, 6Y9Q: PDZ3+taperin peptide

AUTHOR CONTRIBUTIONS

Concept: Y.Z., F.D. and N.W.;
Methodology: Y.Z., F.D. and N.W.;
Protein production: Y.Z.;
Hold-up and SPR: V.G., F.D., E.P., A.B. and S.H.;
Phage display: S.L and Y.I.;
NMR: Y.Z. and F.C.;
AUC and SAXS: Y.Z., C.G. S.B., B.R. and N.W.;
Crystallography and refinement: Y.Z., A.M., and A.H.
Writing – Original Draft: Y.Z. and N.W.;
Writing – Review & Editing: Y.Z., F.D., F.C., B.C-C., C.C., S.B., B.R., A.M., A.H., Y.I., A.B., S.H., and N.W.;
Fundraising: N.W.;

ACKNOWLEDGMENTS

The project has received funding from the European Union's Horizon 2020 research and innovation program under the Marie Skłodowska-Curie grant agreement PDZnet No 675341. The authors also acknowledge the Conseil Régional d'Ile de France for financial support through the SESAME 2014 NMRCHR program No. 14014526 (800 MHz spectrometer).

The authors acknowledge Marie-Christine Vaney for technical assistance concerning the analysis of X-ray diffraction data and Patrick England for technical assistance in SPR experimental design and analysis. The authors are grateful to Sylvie Nouaille for providing the initial plasmid encoding for PDZ3 Δ PBM of whirlin. We acknowledge SOLEIL and ESRF for provision of synchrotron radiation facilities, and we would like to thank the staff of the SWING and PROXIMA1&2 beamlines in synchrotron SOLEIL and ESRF-ID29 beamline for assistance during the SAXS and X-ray diffractions measurements.

References:

- 1 [1] E. Pepermans, V. Michel, R. Goodyear, C. Bonnet, S. Abdi, T. Dupont, S. Gherbi, M.
2 Holder, M. Makrelouf, J.-P. Hardelin, S. Marlin, A. Zenati, G. Richardson, P. Avan, A.
3 Bahloul, C. Petit, The CD2 isoform of protocadherin-15 is an essential component
4 of the tip-link complex in mature auditory hair cells, *EMBO Mol. Med.* 6 (2014)
5 984–992. <https://doi.org/10.15252/emmm.201403976>.
6
7 [2] P. Kazmierczak, H. Sakaguchi, J. Tokita, E.M. Wilson-Kubalek, R.A. Milligan, U.
8 Müller, B. Kachar, Cadherin 23 and protocadherin 15 interact to form tip-link
9 filaments in sensory hair cells, *Nature.* 449 (2007) 87–91.
10 <https://doi.org/10.1038/nature06091>.
11
12 [3] M. Schwander, B. Kachar, U. Müller, The cell biology of hearing, *J. Cell Biol.* 190
13 (2010) 9–20. <https://doi.org/10.1083/jcb.201001138>.
14
15 [4] P. Mathur, J. Yang, Usher syndrome: Hearing loss, retinal degeneration and
16 associated abnormalities, *Biochim. Biophys. Acta - Mol. Basis Dis.* 1852 (2015)
17 406–420. <https://doi.org/10.1016/j.bbadis.2014.11.020>.
18
19 [5] K. Siletti, B. Tarchini, A.J. Hudspeth, Daple coordinates organ-wide and cell-
20 intrinsic polarity to pattern inner-ear hair bundles, *Proc. Natl. Acad. Sci.* 114
21 (2017) E11170–E11179. <https://doi.org/10.1073/pnas.1716522115>.
22
23 [6] R.J. Goodyear, W. Marcotti, C.J. Kros, G.P. Richardson, Development and properties
24 of stereociliary link types in hair cells of the mouse cochlea, *J. Comp. Neurol.* 485
25 (2005) 75–85. <https://doi.org/10.1002/cne.20513>.
26
27 [7] P. Mburu, M. Mustapha, A. Varela, D. Weil, A. El-Amraoui, R.H. Holme, A. Rump, R.E.
28 Hardisty, S. Blanchard, R.S. Coimbra, I. Perfettini, N. Parkinson, A.M. Mallon, P.
29 Glenister, M.J. Rogers, A.J. Paige, L. Moir, J. Clay, A. Rosenthal, X.Z. Liu, G. Blanco,
30 K.P. Steel, C. Petit, S.D.M. Brown, Defects in whirlin, a PDZ domain molecule
31 involved in stereocilia elongation, cause deafness in the whirler mouse and
32 families with DFNB31, *Nat. Genet.* 34 (2003) 421–428.
33 <https://doi.org/10.1038/ng1208>.
34
35 [8] D. Weil, A. El-Amraoui, S. Masmoudi, M. Mustapha, Y. Kikkawa, S. Lainé, S.
36 Delmaghani, A. Adato, S. Nadifi, Z. Ben Zina, C. Hamel, A. Gal, H. Ayadi, H.
37 Yonekawa, C. Petit, Usher syndrome type I G (USH1G) is caused by mutations in
38 the gene encoding SANS, a protein that associates with the USH1C protein,
39 harmonin, *Hum. Mol. Genet.* 12 (2003) 463–471.
40 <https://doi.org/10.1093/hmg/ddg051>.
41
42 [9] I. Ebermann, H.P.N. Scholl, P. Charbel Issa, E. Becirovic, J. Lamprecht, B. Jurkies,
43 J.M. Millán, E. Aller, D. Mitter, H. Bolz, A novel gene for Usher syndrome type 2:
44 Mutations in the long isoform of whirlin are associated with retinitis pigmentosa
45 and sensorineural hearing loss, *Hum. Genet.* 121 (2007) 203–211.
46 <https://doi.org/10.1007/s00439-006-0304-0>.
47
48 [10] N. Michalski, V. Michel, A. Bahloul, H. Yagi, D. Weil, P. Martin, J. Hardelin, M. Sato, C.
49 Petit, Molecular Characterization of the Ankle-Link Complex in Cochlear Hair Cells
50 and Its Role in the Hair Bundle Functioning, 27 (2007) 6478–6488.
51 <https://doi.org/10.1523/JNEUROSCI.0342-07.2007>.
52
53 [11] M. Mustapha, E. Chouery, S. Chardenoux, M. Naboulsi, J. Paronnaud, A. Lemainque,
54 A. Mégarbané, J. Loiselet, D. Weil, M. Lathrop, C. Petit, DFNB31, a recessive form of
55 sensorineural hearing loss, maps to chromosome 9q32-34, *Eur. J. Hum. Genet.* 10
56 (2002) 210–212. <https://doi.org/10.1038/sj/ejhg/5200780>.
57
58 [12] F. Delhommel, F. Cordier, B. Bardiaux, G. Bouvier, B. Colcombet-Cazenave, S. Brier,
59 B. Raynal, S. Nouaille, A. Bahloul, J. Chamot-Rooke, M. Nilges, C. Petit, N. Wolff,
60
61
62
63
64
65

1 Structural Characterization of Whirlin Reveals an Unexpected and Dynamic
2 Supramodule Conformation of Its PDZ Tandem, Structure. 25 (2017) 1645-
3 1656.e5. <https://doi.org/10.1016/j.str.2017.08.013>.

- 4 [13] P.D. Mathur, J. Zou, T. Zheng, A. Almishaal, Y. Wang, Q. Chen, L. Wang, D. Vashist, S.
5 Brown, A. Park, J. Yang, Distinct expression and function of whirlin isoforms in the
6 inner ear and retina: An insight into pathogenesis of USH2D and DFNB31, Hum.
7 Mol. Genet. 24 (2015) 6213–6228. <https://doi.org/10.1093/hmg/ddv339>.
- 8 [14] B. Delprat, V. Michel, R. Goodyear, Y. Yamasaki, N. Michalski, A. El-Amaraoui, I.
9 Perfettini, P. Legrain, G. Richardson, J.P. Hardelin, C. Petit, Myosin XVa and whirlin,
10 two deafness gene products required for hair bundle growth, are located at the
11 stereocilia tips and interact directly, Hum. Mol. Genet. 14 (2005) 401–410.
12 <https://doi.org/10.1093/hmg/ddi036>.
- 13 [15] U. Manor, A. Disanza, M. Grati, L. Andrade, H. Lin, P.P. Di Fiore, G. Scita, B. Kachar,
14 Regulation of stereocilia length by myosin XVa and whirlin depends on the actin-
15 regulatory protein Eps8, Curr. Biol. 21 (2011) 167–172.
16 <https://doi.org/10.1016/j.cub.2010.12.046>.
- 17 [16] S. Ebrahim, N.J. Ingham, M.A. Lewis, M.J.C. Rogers, R. Cui, B. Kachar, J.C. Pass, K.P.
18 Steel, Alternative Splice Forms Influence Functions of Whirlin in Mechanosensory
19 Hair Cell Stereocilia, Cell Rep. 15 (2016) 935–943.
20 <https://doi.org/10.1016/j.celrep.2016.03.081>.
- 21 [17] A. Adato, B. Delprat, V. Michel, N. Michalski, D. Weil, A. El-amraoui, C. Petit, Usherin
22 , the defective protein in Usher syndrome type IIA , is likely to be a component of
23 interstereocilia ankle links in the inner ear sensory cells, 14 (2005) 3921–3932.
24 <https://doi.org/10.1093/hmg/ddi416>.
- 25 [18] I.A. Belyantseva, E.T. Boger, S. Naz, G.I. Frolenkov, J.R. Sellers, Z.M. Ahmed, A.J.
26 Griffith, T.B. Friedman, Myosin-XVa is required for tip localization of whirlin and
27 differential elongation of hair-cell stereocilia, Nat. Cell Biol. 7 (2005) 148–156.
28 <https://doi.org/10.1038/ncb1219>.
- 29 [19] S.A. Mauriac, Y.E. Hien, J.E. Bird, S.D.S. Carvalho, R. Peyroutou, S.C. Lee, M.M.
30 Moreau, J.M. Blanc, A. Geysler, C. Medina, O. Thoumine, S. Beer-Hammer, T.B.
31 Friedman, L. Rüttiger, A. Forge, B. Nürnberg, N. Sans, M. Montcouquiol, Defective
32 Gpsm2/Gai3 signalling disrupts stereocilia development and growth cone actin
33 dynamics in Chudley-McCullough syndrome, Nat. Commun. 8 (2017).
34 <https://doi.org/10.1038/ncomms14907>.
- 35 [20] N. Soroush, K. Baub, J. Plutniok, A. Samanta, B. Knapp, K. Nagel-Wolfrum, U.
36 Wolfrum, Characterization of the ternary Usher syndrome SANS/ush2a/whirlin
37 protein complex, Hum. Mol. Genet. 26 (2017) 1157–1172.
38 <https://doi.org/10.1093/hmg/ddx027>.
- 39 [21] J. Reiners, B. Reidel, A. El-Amraoui, B. Boëda, I. Huber, C. Petit, U. Wolfrum,
40 Differential Distribution of Harmonin Isoforms and Their Possible Role in Usher-1
41 Protein Complexes in Mammalian Photoreceptor Cells, Investig. Ophthalmol. Vis.
42 Sci. 44 (2003) 5006–5015. <https://doi.org/10.1167/iovs.03-0483>.
- 43 [22] B.Z. Harris, W.A. Lim, Mechanism and role of PDZ domains in signaling complex
44 assembly, (2001).
- 45 [23] F. Delhommel, N. Wolff, F. Cordier, 1H, 13C and 15N backbone resonance
46 assignments and dynamic properties of the PDZ tandem of Whirlin, Biomol. NMR
47 Assign. 10 (2016) 361–365. <https://doi.org/10.1007/s12104-016-9701-z>.
- 48 [24] C.C. Yap, F. Liang, Y. Yamazaki, Y. Muto, H. Kishida, T. Hayashida, T. Hashikawa, R.
49 Yano, CIP98, a novel PDZ domain protein, is expressed in the central nervous
50 system.

- system and interacts with calmodulin-dependent serine kinase., *J. Neurochem.* 85 (2003) 123–34. <https://doi.org/10.1046/j.1471-4159.2003.01647.x>.
- [25] P. Mburu, Y. Kikkawa, S. Townsend, R. Romero, H. Yonekawa, S.D.M. Brown, Whirlin complexes with p55 at the stereocilia tip during hair cell development., *Proc. Natl. Acad. Sci. U. S. A.* 103 (2006) 10973–8. <https://doi.org/10.1073/pnas.0600923103>.
- [26] I. Gosens, E. van Wijk, F.F.J. Kersten, E. Krieger, B. van der Zwaag, T. M??rker, S.J.F. Letteboer, S. Dusseljee, T. Peters, H.A. Spierenburg, I.M. Punte, U. Wolfrum, F.P.M. Cremers, H. Kremer, R. Roepman, MPP1 links the Usher protein network and the Crumbs protein complex in the retina, *Hum. Mol. Genet.* 16 (2007) 1993–2003. <https://doi.org/10.1093/hmg/ddm147>.
- [27] R. Vincentelli, K. Luck, J. Poirson, J. Polanowska, J. Abdat, M. Blémont, J. Turchetto, F. Iv, K. Ricquier, M.L. Straub, A. Forster, P. Cassonnet, J.P. Borg, Y. Jacob, M. Masson, Y. Nominé, J. Reboul, N. Wolff, S. Charbonnier, G. Travé, Quantifying domain-ligand affinities and specificities by high-throughput holdup assay, *Nat. Methods.* 12 (2015) 787–793. <https://doi.org/10.1038/nmeth.3438>.
- [28] Z. Dosztányi, Prediction of protein disorder based on IUPred, *Protein Sci.* 27 (2018) 331–340. <https://doi.org/10.1002/pro.3334>.
- [29] F. Delhommel, F. Cordier, F. Saul, L. Chataigner, N. Wolff, Structural plasticity of the HDD2 domain of whirlin, 285 (2018) 3738–3752. <https://doi.org/10.1111/febs.14614>.
- [30] Y. Zhang, B.A. Appleton, C. Wiesmann, T. Lau, M. Costa, R.N. Hannoush, S.S. Sidhu, Inhibition of Wnt signaling by Dishevelled PDZ peptides, 5 (2009) 217–219. <https://doi.org/10.1038/nchembio.152>.
- [31] R.R. Penkert, H.M. DiVittorio, K.E. Prehoda, Internal recognition through PDZ domain plasticity in the Par-6-Pals1 complex, *Nat. Struct. Mol. Biol.* 11 (2004) 1122–1127. <https://doi.org/10.1038/nsmb839>.
- [32] B.J. Hillier, K.S. Christopherson, K.E. Prehoda, D.S. Bredt, W.A. Lim, Unexpected modes of PDZ domain scaffolding revealed by structure of nNOS-syntrophin complex, *Science (80-.)*. 284 (1999) 812–815. <https://doi.org/10.1126/science.284.5415.812>.
- [33] N.E. Davey, M.H. Seo, V.K. Yadav, J. Jeon, S. Nim, I. Krystkowiak, C. Blikstad, D. Dong, N. Markova, P.M. Kim, Y. Ivarsson, Discovery of short linear motif-mediated interactions through phage display of intrinsically disordered regions of the human proteome, *FEBS J.* 284 (2017) 485–498. <https://doi.org/10.1111/febs.13995>.
- [34] A.U. Rehman, R.J. Morell, I.A. Belyantseva, S.Y. Khan, E.T. Boger, M. Shahzad, Z.M. Ahmed, S. Riazuddin, S.N. Khan, S. Riazuddin, T.B. Friedman, Targeted Capture and Next-Generation Sequencing Identifies C9orf75, Encoding Taperin, as the Mutated Gene in Nonsyndromic Deafness DFNB79, *Am. J. Hum. Genet.* 86 (2010) 378–388. <https://doi.org/10.1016/j.ajhg.2010.01.030>.
- [35] M. Chen, Q. Wang, G.H. Zhu, P. Hu, Y. Zhou, T. Wang, R.S. Lai, Z.A. Xiao, D.H. Xie, Progressive hearing loss and degeneration of hair cell stereocilia in taperin gene knockout mice, *Biochem. Biophys. Res. Commun.* 479 (2016) 703–707. <https://doi.org/10.1016/j.bbrc.2016.09.148>.
- [36] B. Zhao, Z. Wu, U. Mu, C. Neuroscience, L. Jolla, U. States, T. Scripps, L. Jolla, U. States, Murine Fam65b forms ring-like structures at the base of stereocilia critical for mechanosensory hair cell function, (2016) 1–24. <https://doi.org/10.7554/eLife.14222>.

- 1
2
3
4
5
6
7
8
9
10
11
12
13
14
15
16
17
18
19
20
21
22
23
24
25
26
27
28
29
30
31
32
33
34
35
36
37
38
39
40
41
42
43
44
45
46
47
48
49
50
51
52
53
54
55
56
57
58
59
60
61
62
63
64
65
- [37] P. Maisonneuve, C. Caillet-Saguy, M.C. Vaney, E. Bibi-Zainab, K. Sawyer, B. Raynal, A. Haouz, M. Delepierre, M. Lafon, F. Cordier, N. Wolff, Molecular basis of the interaction of the human protein tyrosine phosphatase non-receptor type 4 (PTPN4) with the mitogen-activated protein kinase p38 γ , *J. Biol. Chem.* 291 (2016) 16699–16708. <https://doi.org/10.1074/jbc.M115.707208>.
- [38] G. Lipari, A. Szabo, Model-free approach to the interpretation of nuclear magnetic resonance relaxation in macromolecules, *J. Am. Chem. Soc.* 104 (1982) 4546–4559.
- [39] N.J. Zondlo, Aromatic-proline interactions: Electronically tunable CH/ π interactions, *Acc. Chem. Res.* 46 (2013) 1039–1049. <https://doi.org/10.1021/ar300087y>.
- [40] Y. Mu, P. Cai, S. Hu, S. Ma, Y. Gao, Characterization of diverse internal binding specificities of PDZ domains by yeast two-hybrid screening of a special peptide library, *PLoS One.* 9 (2014). <https://doi.org/10.1371/journal.pone.0088286>.
- [41] E. van Wijk, B. van der Zwaag, T. Peters, U. Zimmermann, H. te Brinke, F.F.J. Kersten, T. Märker, E. Aller, L.H. Hoefsloot, C.W.R.J. Cremers, F.P.M. Cremers, U. Wolfrum, M. Knipper, R. Roepman, H. Kremer, The DFNB31 gene product whirlin connects to the Usher protein network in the cochlea and retina by direct association with USH2A and VLGR1, *Hum. Mol. Genet.* 15 (2006) 751–765. <https://doi.org/10.1093/hmg/ddi490>.
- [42] F.F.J. Kersten, E. van Wijk, J. van Reeuwijk, B. van der Zwaag, T. Märker, T.A. Peters, N. Katsanis, U. Wolfrum, J.E.E. Keunen, R. Roepman, H. Kremer, Association of whirlin with Cav1.3 (α 1D) channels in photoreceptors, defining a novel member of the usher protein network, *Investig. Ophthalmol. Vis. Sci.* 51 (2010) 2338–2346. <https://doi.org/10.1167/iovs.09-4650>.
- [43] J.C. de Nooij, C.M. Simon, A. Simon, S. Doobar, K.P. Steel, R.W. Banks, G.Z. Mentis, G.S. Bewick, T.M. Jessell, The PDZ-Domain Protein Whirlin Facilitates Mechanosensory Signaling in Mammalian Proprioceptors, *J. Neurosci.* 35 (2015) 3073–3084. <https://doi.org/10.1523/JNEUROSCI.3699-14.2015>.
- [44] O.N. Rogacheva, S.A. Izmailov, L. V. Slipchenko, N.R. Skrynnikov, A new structural arrangement in proteins involving lysine NH₃⁺ group and carbonyl, *Sci. Rep.* 7 (2017) 1–8. <https://doi.org/10.1038/s41598-017-16584-y>.
- [45] S.K. Burley, G.A. Petsko, Aromatic-aromatic interaction: A mechanism of protein structure stabilization, *Science* (80-.). 229 (1985) 23–28. <https://doi.org/10.1126/science.3892686>.
- [46] S.M. Butterfield, P.R. Patel, M.L. Waters, Contribution of aromatic interactions to α -helix stability, *J. Am. Chem. Soc.* 124 (2002) 9751–9755. <https://doi.org/10.1021/ja026668q>.
- [47] K.N.M. Daeffler, H.A. Lester, D.A. Dougherty, Functionally important aromatic-aromatic and sulfur- π interactions in the D2 dopamine receptor, *J. Am. Chem. Soc.* 134 (2012) 14890–14896. <https://doi.org/10.1021/ja304560x>.
- [48] U. Samanta, D. Pal, P. Chakrabarti, Packing of aromatic rings against tryptophan residues in proteins, (1999) 1421–1427. <https://doi.org/10.1107/S090744499900726X>.
- [49] Q. Chen, J. Zou, Z. Shen, W. Zhang, J. Yang, Whirlin and PDZ domain-containing 7 (PDZD7) proteins are both required to form the quaternary protein complex associated with Usher syndrome type 2, *J. Biol. Chem.* 289 (2014) 36070–36088. <https://doi.org/10.1074/jbc.M114.610535>.